J Porous Mater (2007) 14:61–69
DOI 10.1007/s10934-006-9009-y

Atomic force microscopy (AFM) characterisation of the porous silica nanostructure of two centric diatoms

Dusan Losic · Rachel J. Pillar · Thorsten Dilger · James G. Mitchell · Nicolas H. Voelcker

Received: 4 October 2005 / Revised: 27 January 2006 / Published online: 6 December 2006

Abstract The porous silica nanostructure of two marine, centric diatoms, *Coscinodiscus* sp. and *Thalassiosira eccentrica* was investigated by atomic force microscopy (AFM). Important morphological features of the silica frustules of diatoms are described, including: the organisation of porous silica layers, their topography, pore size, shape and density. The outer layer of *Coscinodiscus* sp., commonly called the cribellum, consists of a characteristic hexagonal array of pores with pore sizes of around 45 nm. This thin membrane covers a second structural layer where two different silica surfaces are identified. The outer part, known as the cribrum consists of hexagonally packed pores of about 200 nm diameter. The inner part, known as the foramen layer, consists of larger and radially distributed holes with a diameter of around 1,150 nm. The second diatom species investigated, *T. eccentrica* produces a frustule with one silica structural layer featuring two different porous surfaces. The outer surface has large (800 nm diameter) holes (foramen) while the inner surface contains a porous wall with pores comparable in size to the *Coscinodiscus* sp. cribellum. The inner and outer surfaces of the frustule wall of both diatoms are hence in reverse order. However, the size of the small pores is similar for both species. High-resolution AFM also revealed the granular nanostructure of the diatom biosilica with grain sizes from 20 to 70 nm diameters.

Keywords Atomic force microscopy · Biomineralisation · Biosilica · Porous membranes · Diatoms

D. Losic (✉) · R. J. Pillar · T. Dilger · N. H. Voelcker
School of Chemistry, Physics and Earth Science, Flinders University, Adelaide 5001, Australia
e-mail: dusan.losic@flinders.edu.au

D. Losic · J. G. Mitchell
School of Biological Sciences, Flinders University, Adelaide 5001, Australia

1 Introduction

There is a great interest in the science and technology of gaining inspiration from nature for the design and manufacture of nanostructured materials [1–3]. Biomaterials made through the process of biomineralisation are highly controlled from the molecular level to the nanoscale and the macroscopic level resulting in complex bioinorganic architectures [4]. Understanding the processes involved in biomineralisation may eventually allow mimicking these structures and producing new materials with advanced mechanical, magnetic, optical, electrical, piezoelectrical, or adhesive properties [4–9].

The unicellular algae known as diatoms are outstanding examples of micro- and nanostructured materials in nature [10]. They produce exceptional three-dimensional silica scaffolds, which have great potential for nanotechnological applications [6, 7, 9]. The diversity of their structures is extraordinary with about 10,000 species, each with unique silica morphology ranging from nanometres to micrometres [10, 11]. Their main morphological feature is the frustule, a silica cell wall that consists of two valves, encasing the protoplasm, joined together by siliceous girdle bands. A schematic diagram of a common frustule structure of

centric diatoms is shown in Fig. 1A. The frustule of two marine diatoms species were investigated in this work: *Coscinodiscus* sp. and *T. eccentrica.* SEM images in Fig. 1B and C show the forms of their frustule valves. The frustule of centric diatoms consists of a honeycomb of hexagonal chambers, called areolae. In general, each chamber has an outer surface, exposed to the external environment and an inner surface. One of the two surfaces is perforated by large, round holes called foramen, while the other surfaces contain one or two silica plates (cribellum and cribrum) perforated by a complex and highly symmetrical pore arrangement (sieve plate) [10, 11].

The technological importance of diatoms has been the subject of a series of recent reviews on the interface of nano- and biotechnology [3, 9, 12]. Applications as advanced material in filtration systems such as gel filtration, immunoisolation, biosensing, optoelectronics and as templates for fabrication on nanomaterials have been proposed [6, 7, 13–15]. Diatoms can routinely be grown to more than million cells per ml of culture medium, which offers the possibility of cheap production of nanostructured silica. In our previous work, we have shown that the microtopography of diatom surfaces controls particle movement in very specific manners that appear consistent with surface-induced drag [16–18]. The surface structure alters the diffusion and advection of submicrometre particles, resulting in localised concentrations of particles on ridged areas surrounding the areolar chambers. Detailed understanding of successful particle sorting by diatoms may reveal principles and concepts that will be extremely useful when designing micro- and nano-fluidic components in lab-on-a-chip systems [19].

Diverse analytical tools have been used for the characterisation of diatom frustules including scanning electron microscopy (SEM), transmission electron microscopy (TEM), confocal microscopy, atomic force microscopy (AFM), Fourier transform infrared spectroscopy (FTIR), X-ray scattering (SAXS), and X-ray photoelectron spectroscopy (XPS) [20–25]. Traditionally, SEM and TEM are most frequently used in the study of diatom morphology and taxonomy. However, AFM based studies offer significant advantages like: imaging with minimum sample preparation (conductive layer is not required), higher resolution, ability to measure structural and micromechanical properties (hardness, adhesivity and elasticity) and the potential of imaging live diatoms in aqueous medium [22–28]. Several AFM studies of the topographical and mechanical properties of various diatom species have recently been reported [22–24]. In the present work, we have used AFM to investigate the frustule topography of two diatoms species *Coscinodiscus* sp. and *T. eccentrica.* Both of these diatoms have fascinating silica structures and to our knowledge this is the first

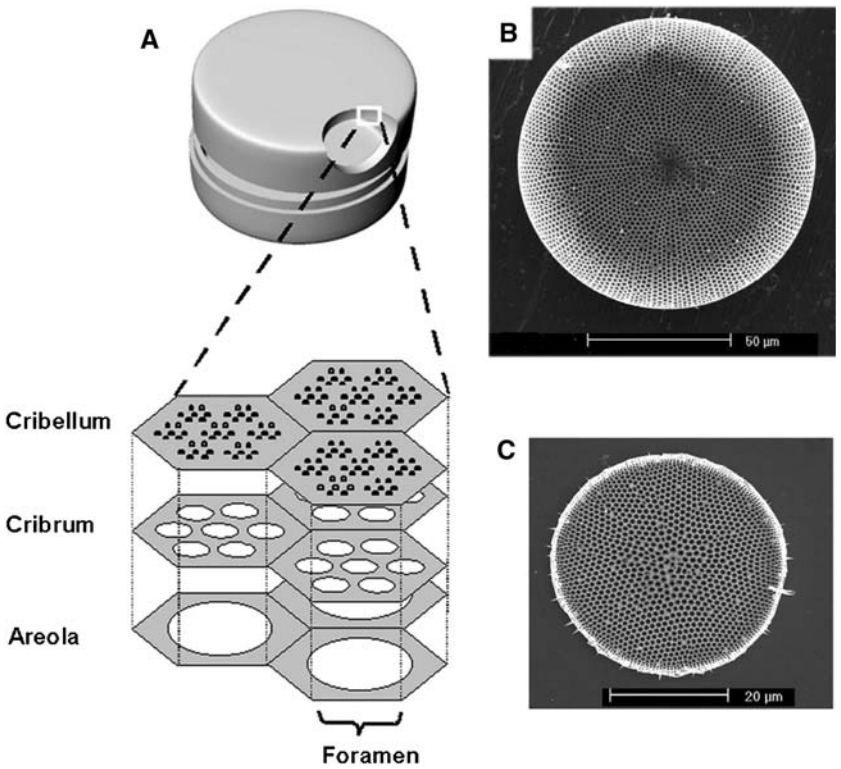

Fig. 1 (**A**) Schematic of a centric diatom frustule with cross-sectional profile of the silica wall based on SEM data. The inner layer with honeycomb-like chambers called areolae with large holes in the silica plate are known as foramen. The roof of the areolae is called the cribrum, which contains a regular pattern of pores. The layer over the cribrum is a thin siliceous membrane known as cribellum, which consists small pores. (**B**) SEM image of a *Coscinodiscus* sp. frustule and (**C**) SEM image of *T. eccentrica*

AFM study of these species. The focus of this study is to obtain detailed information about porous biosilica nanostructures and higher resolution images of outer and inner frustule membranes than are possible using SEM. Better understanding of the diatom frustule structure from the nanometre scale up to whole cell will provide new insight of the process of silica biomineralisation in diatoms, explain still unknown functions of porous biosilica membranes and anticipate potential technological applications.

2 Materials and methods

Coscinodiscus sp. and *Thalassiosira eccentrica* were obtained from CSIRO, Marine Research (Hobart, Tasmania, Australia). The cultures were maintained at 20 °C using a 12 h light/12 h dark cycle. GSE medium was used to culture *Coscinodiscus* sp. and Guillard's medium (f/2) was used for *T. eccentrica* [29]. The live diatoms were harvested after 2–3 weeks of culturing and cleaned using a procedure described elsewhere [30]. Organic materials from the frustule surface was removed by treatment with concentrated sulphuric acid with small quantities of saturated potassium permanganate and oxalic acid. More gentle cleaning was performed using 2% SDS in 100 mM EDTA solution [11]. Cleaned diatoms were stored in ethanol (100%). To investigate the topography of the frustule surface by AFM, one drop of cleaned cell suspensions was deposited on freshly cleaved mica or silicon wafers previously modified with 0.01% polylysine. Samples were dried in a stream of nitrogen for 1 min. Diatoms were imaged with intact and separated frustules. Frustules settled on the substrate surface exposing their interior surface (concave) or exterior surface (convex).

For SEM studies, cleaned diatoms were deposited on mica or silicon, coated with a thin platinum layer and mounted on microscopy stubs with carbon sticky tape. The images were acquired using a Philips XL 30 field-emission scanning electron microscope operated at 2–10 kV.

AFM imaging of prepared diatoms was performed using a Nanoscope IV Multimode SPM (Veeco Corp, Santa Barbara, USA). Images were acquired in air using contact and tapping modes. Oxide-sharpened silicon nitride probes (NP-S, Veeco Corp, Santa Barbara, USA) of spring constant $k = 0.15$ N/m were used in contact mode experiments. Olympus silicon probes (TESP, Veeco Corp, Santa Barbara, USA) were used for imaging in tapping mode. AFM tips were characterised using silicon calibrating grating (TGT01, supplied by MikroMasch, Silicon-MDT Ltd., Russia) as described in previous work to determine their sharpness parameters (aspect ratio and curvature radius) [31]. Different parts of the frustule from the central to the peripheral areas were scanned on the inner and outer frustule surface. For each sample, height, phase (tapping mode) and deflection images were recorded. Height images are presented here unless stated otherwise. The contact force applied to each sample was minimised to avoid tip-induced damage to the membranes, except for experiments where the frustule was deliberately indented or fractured. Samples were scanned slowly due to the large vertical range of topographical features (up to 0.7 μm in z). A minimum of 10 different frustules of each species was imaged to account for minor shape variations. All values given are the average of at least 50 individual measurements performed on at least 5 different frustules ± the standard deviation. Image processing (''bearing'', grain size, roughness (R_a) and profile analysis) was performed using DI off-line software (Veeco Corp. Santa Barbara, USA) and SPIP software (Image Metrology, Denmark).

3 Results and discussion

3.1 AFM imaging of *Coscinodiscus* sp.

A typical topographic AFM image of the cribellum layer, which represents the outermost surface of *Coscinodiscus* sp. is shown in Fig. 2A and B. This surface features a hillock topography with about 2 μm wide porous domes arranged on the surface in hexagonal packing. A comparative SEM image (Fig. 2C) shows similar pore organisation. Although domes can also be seen in SEM, they are not as obvious as in AFM images, presumably due to their small height and lack of backscattering contrast in SEM. A more detailed AFM image of this dome structure is presented in Fig. 2D. The basic feature of this silica structure is an array of 5–7 small pores with about 20 arrays per dome arranged in a roughly hexagonal lattice. These arrays average 195 ± 15 nm in diameter. The distance between arrays was 180 ± 37 nm. Within each array, 4–6 pores are generally arranged around a central pore (Fig. 2E). An AFM image of a typical array with its corresponding cross-section is shown in Fig. 2E and F. Both circular and irregular shaped pores were observed, with diameters of 45 ± 9 nm and a pore-to-pore distance of 68 ± 12 nm. The porosity of this layer was determined as 7.5 ± 1.5%. High-resolution AFM images of cribellum layer show presence of small silica

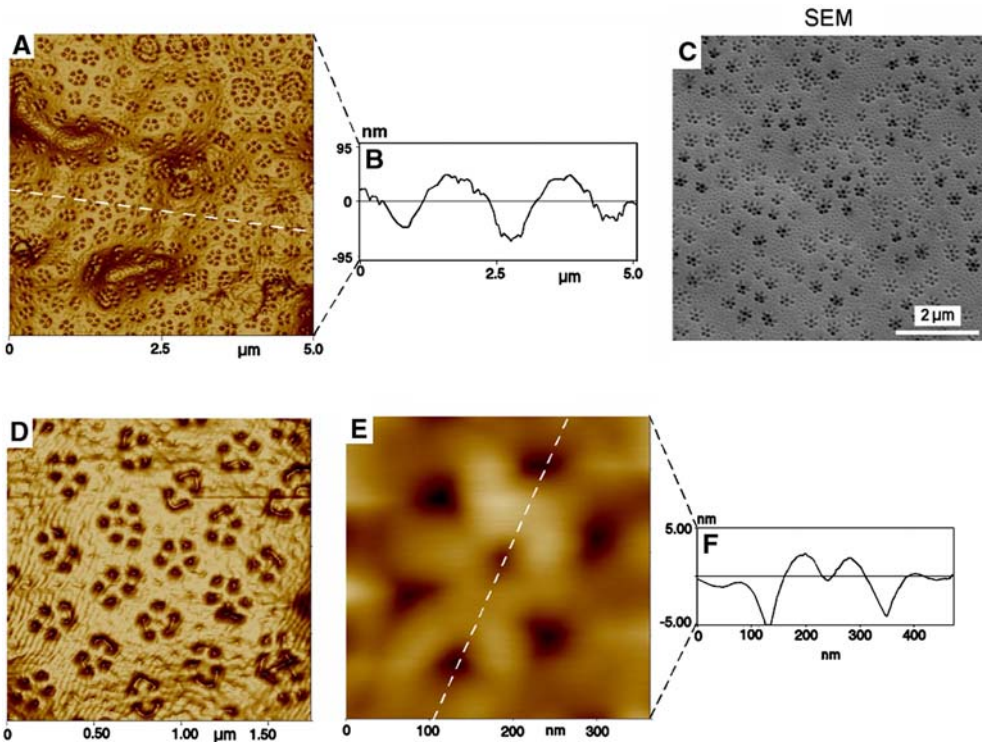

Fig. 2 Outer surface (cribellum) of *Coscinodiscus* sp. (**A**) AFM image (tapping mode in air) of the cribellum surface showing porous domes forming hillock topography. Corresponding cross-section graph in (**B**). (**C**) Comparative SEM image of cribellum surface. (**D**) Enlarged AFM image of a single dome shows details of pore organisation, *z*-range 100 nm. (**E**) High resolution AFM image of one typical hexagonal pore array and (**F**) corresponding cross-section graph

nodules with size of 35 ± 4 nm. Their surface roughness (R_a) was 2.5 ± 0.4 nm (measured on 200 × 200 nm area). This cribellum layer represents the outer sieve plate layer in contact with the external environment. Hence its structural features like general topography, pore size, pore organisation and density are important for nutrient uptake, sorting nutrients, and defence against bacterial and viral attack. The observed pore size suggests that this layer can successfully act as mechanical barrier or filter that allows passage for particles smaller than 45 nm which are unlikely to be of viral nature and more likely to be salubrious. The function of the wave-like topography of the domes and the hexagonal organisation scaled from top (domes) to bottom (arrays and pores) remains to be elucidated.

The cribellum of *Coscinodiscus* sp. was conserved only for gently cleaned diatoms but rarely on diatoms prepared by the more drastic cleaning procedure using sulphuric acid. This is probably due to the cribellum layer being thin (< 50 nm) and fragile, containing some organic matter and being only weakly bonded to the underlying silica membrane (see below).

Removing the cribellum by acidic cleaning, allows us to investigate the outer surface of the second layer, known as the cribrum. A series of AFM images of this surface is shown in Fig. 3. The large-scale image of the cribrum surface (10 × 10 µm) shows honeycomb topography with domes of 1,620 ± 131 nm diameter arranged to almost perfect hexagons (Fig. 3A). A three-dimensional view and a corresponding cross-section graph of this surface show a hillock profile with a dome height of 52 ± 8 nm and distance between dome tops 1,700 ± 171 nm (Fig. 3B). Although the hillock topography appears both in the cribellum and the cribrum, the cribrum domes have a much more regular shapes and packing. Interestingly, in previous SEM studies these dome structures in the cribrum were observed or interpreted as depressions [16–18]. Our SEM images also show darker porous structures surrounded by light borders, therefore appearing as depressions (Fig 3D). This however is due to the contrast in SEM in this case resulting more from differences in material density than from topographical features. The perforations of the dome-shaped silica membrane are shown in more detail in the AFM image in Fig. 3D, which also reveals occasional 400–500 nm wide holes in between the domes (arrows). These could correspond to imperfections in their structure due to sub-optimal growth conditions, but more likely to mechanical damages to the membrane during cleaning or manipulation. 20 cribrum perforations with a mean diameter of 192 ± 35 nm decorate each dome in average (Fig. 3E, F). The porosity of this layer was 22.5 ± 2.5%. Density and diameter of these pores therefore coincide well with the density and diameter of arrays (ca. 200 nm) on the cribellum layer (Fig. 2D), demonstrating a self-similarity in the observed patterns at the different vertical layers. Although we could not

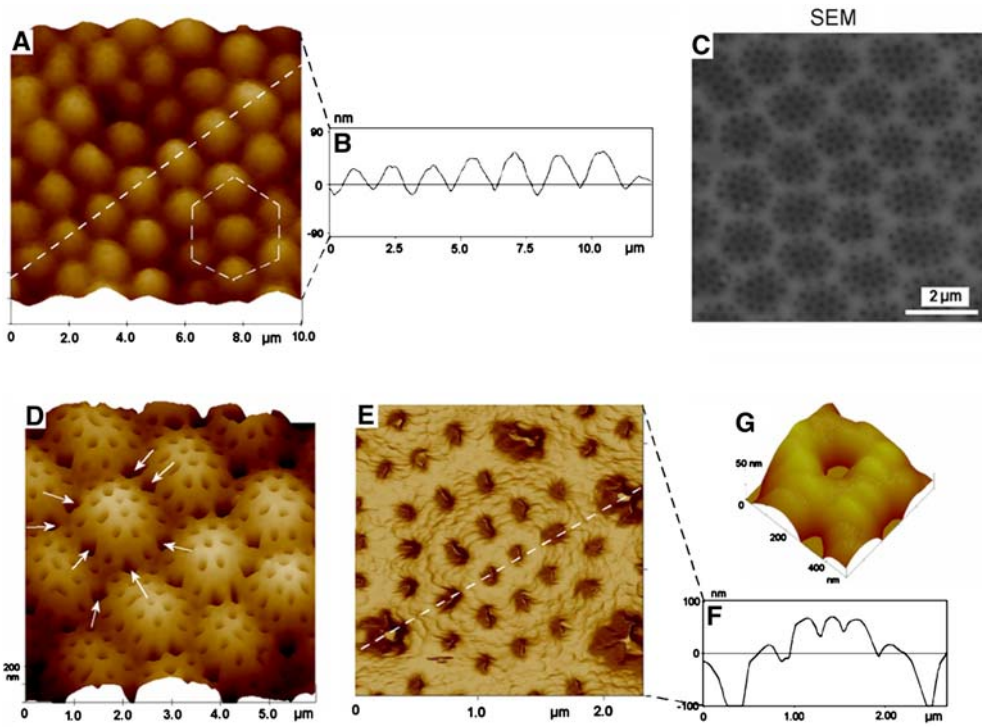

Fig. 3 Cribrum layer of *Coscinodiscus* sp. (**A**) Large scale AFM image (tapping mode in air) of cribrum surface showing a regular honeycomb-like structures. Hexagonal pattern is marked and corresponding cross-section is shown in (**B**). (**C**) Comparative SEM image of cribrum surface, (**D**) AFM image of cribrum in more detail; arrows point to some irregularities between domes. (**E**) Higher resolution AFM image of one dome showing hexagonal organisation and a corresponding cross-section in (**F**). (**G**) Zoom-in showing granular topography of assembled silica nanoparticles

scan the cribellum through the cribrum pores, we believe that the pore areas of cribrum and cribellum are overlaid. This self-consistency is implied in the diagram in Fig. 1B. High-resolution AFM images of cribrum silica material (Fig. 3G) show that the silica consists of silica structures of 74 ± 8 nm diameter, approximately twice the size of the nodulus observed on the cribellum. These presumably stem from colloidal silica nanoparticles incorporated into the growing frustule during biomineralisation [32]. These silica building blocks have not been observed in previous SEM studies of diatom silica.

An AFM image of the inner frustule surface of *Coscinodiscus* sp. is shown in Fig. 4A. A large-scale image (15 × 15 µm) obtained in contact mode shows the presence of hexagonally arranged holes (foramen) of 1,153 ± 131 nm. They are radially organised in lines of 25–35 holes from the cell centre to the frustule edge with a spacing of 603 ± 41 nm. The porosity of this layer was 35 ± 3%, which shows increasing porosity from the outer to the inner membrane. In between foramen holes, long zig-zag channels between holes are apparent (Fig. 4A, arrows) with a width of 160 ± 40 nm and a depth of 29 ± 5 nm. These channels extend radially from the centre of the silica membrane where they are integrated into a large circular plate of 4 µm in diameter (Fig. 4B). This plate is the central part of the diatom structure under which the cell nucleus is located [10]. To date, nothing is known about the function of these channels. Detailed AFM images of the inner frustule surface (Fig. 4D, E) also show that the edges of the foramen are elevated by 75 ± 14 nm. These circular ridges were not seen in SEM micrographs (Fig. 4C). Apart from the channels and ridges, this silica plate is considerably smoother than the cribrum and cribellum. High-resolution image (Fig. 4F) revealed the presence of small silica nodules on the foramen layer with an average diameter of 22 ± 3 nm. The roughness (R_a) of this surface measured from 300 × 300 nm area was 1.4 ± 0.3 nm. These results confirm the lower surface roughness of the internal layer in comparison with external layer (2.5 ± 0.4 nm). Using silicon nitride and contact mode tips, we were unable to image the cribrum layer when probing through the foramen opening (Fig. 4A–D). This is probably due to an insufficient tip aspect ratio (according to the tip specifications given by the supplier). However, when using a slightly higher aspect ratio tapping mode tip, a perforated silica layer could be imaged (Fig. 4G, H). A cross-sectional graph from this image allows us to measure the depth of this layer (359 ± 62 nm) and the dimensions of its perforations. These indeed match the perforations on the outer cribrum surface (Fig. 3D) and a high-resolution AFM image of the inner cribrum silica surface (Fig. 4H) showed a similar morphology of silica nodules to that observed in Fig. 3G.

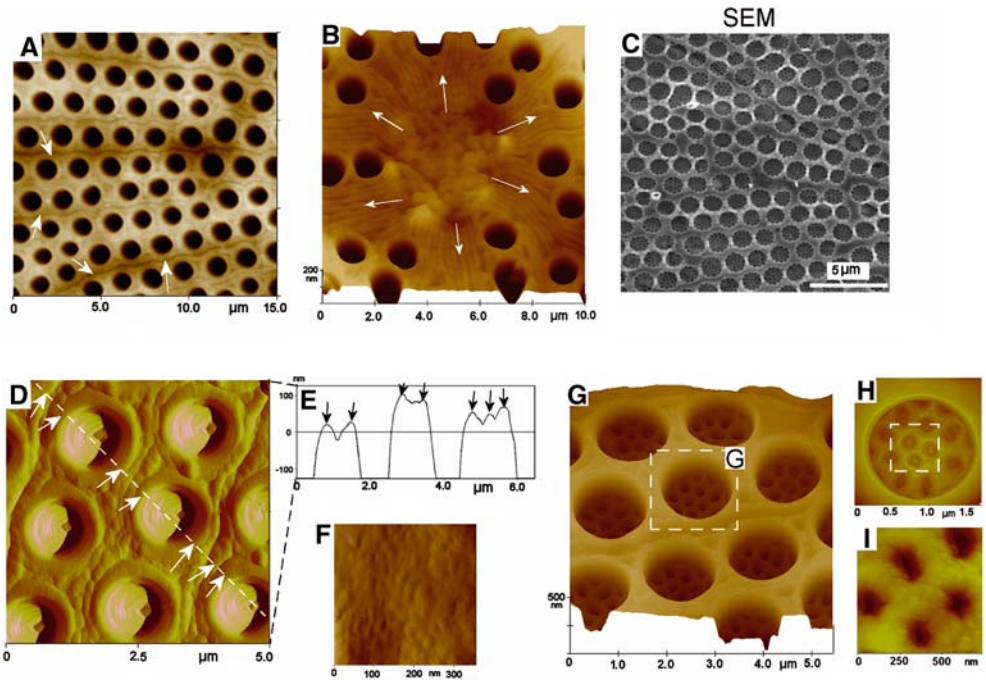

Fig. 4 Inner frustule surface of *Coscinodiscus* sp. (**A**) Contact mode AFM image showing regularly dispersed holes (foramen), *z*-range is 500 nm. Characteristic channels are observed between holes (arrows). (**B**) Contact mode AFM image of central part of frustule with channel joints (arrows). (**C**) Comparative SEM image of inner frustule surface. (**D**) Contact mode AFM image (deflection) and cross-section graph on (**E**) with more details of foramen structures showing characteristic ridges structure on the edge (arrows). (**F**) High resolution tapping mode AFM image of inner surface showing silica nodules. (**G**) Tapping mode AFM image of the inner surface imaged in contact mode depicted in (**A**) showing porous structure of cribrum within a foramen hole. (**H**, **I**) Zoom-ins of one foramen perforation exposing cribrum pores

The robustness of the inner frustule surface was probed by AFM in contact mode applying a force 100 nN on the silica between the foramen openings. The frustule displays good mechanical strength, which is in agreement with recent studies [33]. In one instance, we were able to induce a crack in the silica, but this fracture did not propagate further across the surface. The macroscopic mechanical strength of the frustule is presumably the result of both its pore architecture and the inherent mechanical properties of the nanostructured biosilica [33]. A nanoindentation study of diatom silica will be the subject of a future manuscript.

3.2 AFM imaging of *T. eccentrica*

A series of AFM images of the outer layer of the frustule of *T. eccentrica* is presented in Fig. 5. Typical large-scale images with corresponding cross-sectional graphs are shown in Fig. 5A and B. A comparative SEM image is shown in Fig. 5C. These figures show a membrane perforated by hexagonally packed pores of 770 ± 38 nm diameter, spaced 473 ± 55 nm apart. The porosity of this layer is determined as $37 \pm 3\%$, which is similar to the porosity of the foramen layer for *Coscinodiscus* sp. The outer frustule structure bears resemblance to the inner frustule surface of *Coscinodiscus* sp. (Fig. 4A). However, *T. eccentrica* foramen holes are not radially organised like the foramen on *Coscinodiscus* sp. (Fig. 4). Rather, they follow a concentric arrangement (Fig. 5A). Interestingly, the *T. eccentrica* outer frustule surface was devoid of channels and high-resolution AFM images of this surface (Fig. 5D–F) show that the ridge structures on the edge of the foramen pores are much smaller (15 ± 3 nm) than in *Coscinodiscus* sp. (Fig. 4D). Moreover, in contrast to the relatively smooth foramen of *Coscinodiscus* sp., the foramen silica of *T. eccentrica* has a granular nanostructured topography with the nodules in size of 40 ± 6 nm (Fig. 5D–F). Their surface roughness (R_a) was 4.1 ± 0.5 nm (300×300 nm area). We attempted to image the inner surface at the bottom of areolae, but this could not be achieved due to the steepness of the areolar chambers in *T. eccentrica* and the insufficient aspect ratio of the AFM tips used (obtained from the technical specifications by the supplier).

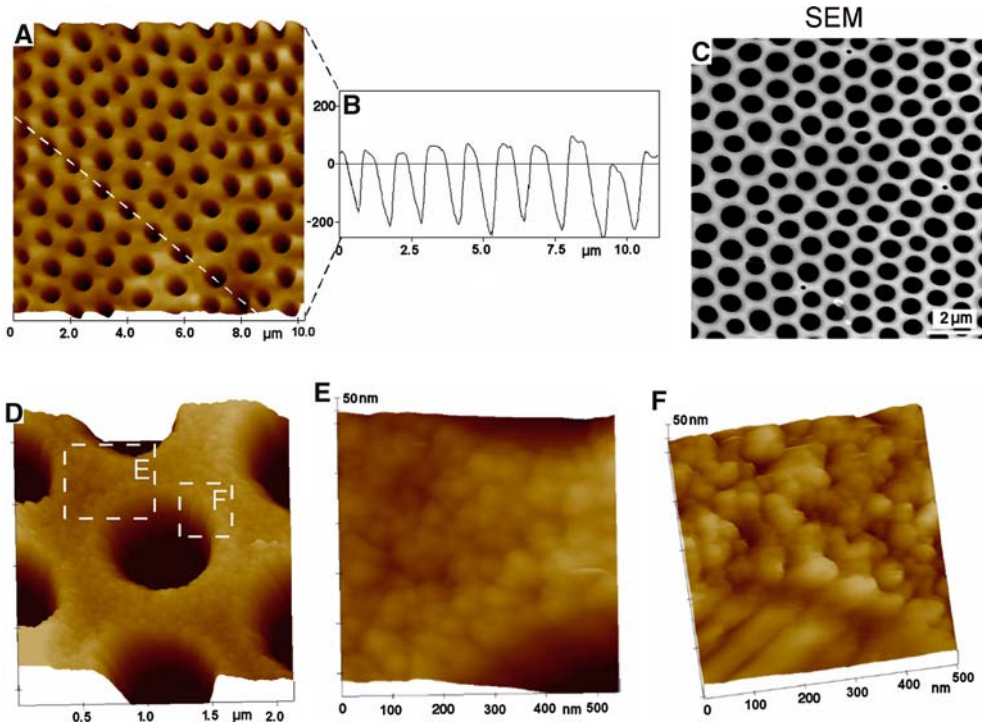

Fig. 5 Outer surface of *T. ecc.* A) Large scale contact mode AFM image shows organisation of holes (foramen), B) Corresponding cross-section graph, C) SEM image of outer surface. D) AFM image of outer surface in more detail, showing hexagonal organisation, z-range is 500 nm. E-F) High resolution tapping mode AFM images of ridge surface between two foramen openings revealing granular topography on the nanoscale

AFM and SEM images of the inner frustule of *T. eccentrica* show a membrane decorated with porous patches arranged in hexagons (Fig. 6A–C). The resulting pattern is centripetal in relation to the arrangement of foramen openings on the outer frustule (Fig. 5A). Figure 6B reveals that these patches of 780 ± 90 nm diameter are slightly recessed by about 10 nm, therefore forming a well. Some wells deviate considerably from the circular shape, and ellipsoidal, quasi-rectangular as well as rhomboidal geometries were commonly observed (Fig. 6D–F) Fusion of these patches was also occasionally seen (Fig. 6G), perhaps due to sub-optimal culture conditions. The pores within the porous areas had a diameter of 43 ± 6 nm, which are similar to the size of the cribellum pores in *Coscinodiscus* sp. and the porosity of this layer (10 ± 2.5%) is similar to the outer layer in *Coscinodiscus* sp. (7.5 ± 1.5%). In the higher magnification AFM image (Fig 6H) and its Fourier transform (inset), the hexagonal packing of the pores within the wells was once again established. However, on occasions, undeveloped pores are visible, particularly in the central part of the wells (Fig. 6A, arrows). High-resolution AFM images and cross-sectional graph (Fig. 6H–J) show that these pore structures are build by silica particles of 50–70 nm diameter. This porous silica layer is similar in morphology but of higher regularity than porous silicon prepared by anodisation of doped silicon [34]. The mechanical strength of this membrane was probed by contact mode AFM. The porous layer was very fragile and could be easily broken by the AFM tip by applying a higher force (> 20 nN) (Fig. 6K). High-resolution AFM images of nonporous surface (between patches) show presence of small silica nodules with average size of 22 ± 2.5. The surface roughness (R_a) was 1.2 ± 0.2 nm (300 × 300 nm area). The inner layer for this specie also shows a smoother surface in comparison with outer layer (4.1 ± 0.5 nm). It was interesting that the size of these silica nodules is double smaller than silica particles seen in porous structure in the same layer. The reason for the observed difference could be explained by requirements for building a stronger porous structure using larger particles.

Several other differences between the frustules of the two species were observed from the AFM images. At 30–40 µm in diameter, *T. eccentrica* are approximately half the size of *Coscinodiscus* sp. The foramen diameter in *T. eccentrica* was about 35% smaller. However, the main differences are the presence of two layers in the *Coscinodiscus* sp. frustule versus one layer in *T. eccentrica* and the inversion of their frustule organisation. Whilst the *Coscinodiscus* sp. frustule pore size decreased from the inside (foramen) to the outside with the cribellum sieves, in *T. eccentrica* the order is reversed and the larger pores were observed on the outer frustule surface and the smaller on the inside.

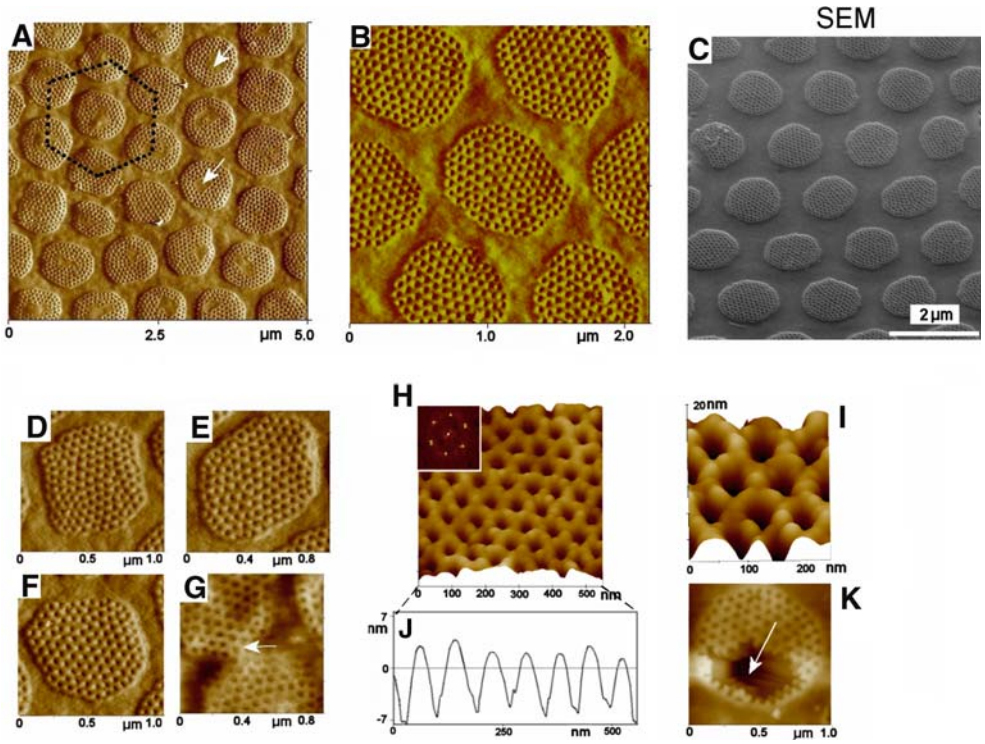

Fig. 6 Inner surface of *T. eccentrica.* (**A**) AFM image shows organisation of circular porous patches organised in hexagonal pattern, *z*-range is 300 nm. (**B**) Higher resolution AFM image of porous well. (**C**) Comparative SEM image of inner surface. (**D–F**) Several different shapes of wells are observed such as square, rhomboidal and quasi circular. (**G**) Example of incomplete separation of wells during frustule formation. (**H** and **I**) High-resolution AFM images of porous well membrane, inset: Fourier transform spectrum. (**J**) Corresponding cross-section graph, and (**K**) Image of porous well after damaging with an AFM tip (arrow)

However, the diameter of the small pores in both cases was about 45 nm, although they are situated on opposite sides of the frustule, suggesting that there is a common function that requires such critical pore size. The organisation of these pores within their respective membrane is again quite different. Pores in *T. eccentrica* are grouped together in large ($N > 100$) arrays. In *Coscinodiscus* sp. pores are organised in smaller arrays of 5–7 pores, which are regularly dispersed across all surface.

4 Conclusions

An AFM investigation of the two centric marine diatoms *Coscinodiscus* sp. and *T. eccentrica* is presented. Our results show that frustule structure could be resolved with great detail at both micro- and nanoscale using AFM. It was demonstrated that the fundamental difference between these two species consists in the inversion of small pore sieve plate and foramen layers. Other morphological differences include the size and geometrical arrangement of frustule features. There is consensus about the size of the smallest pores (45 nm), yet the porosity of their membrane and its position on the frustule was distinct. In biomineralised structures, the structural features are usually optimised for certain functions. In diatoms, the presence of multiple nanostructured membranes and their organisation could assist diatoms to interact in specific ways with their environment by taking up nutrition, for defence or communication.

Some of the observed morphological characteristics were already known from previous SEM studies, but have never been obtained using AFM [10, 11]. But more importantly, high-resolution AFM imaging revealed several new structural features of diatom frustules not reported before:

- The hillock topography of the outside sieve surface (cribellum) of *Coscinodiscus* sp. has not been previously reported. It raises the question about their specific function, some of the possibilities are optimisation of light harvesting, sorting nutrients or movement functions.
- Second, ridge structures around foramen were for the first time observed in this study. Their function is not understood at this point, but ridges might be implicated in the control of submicrometre particle movement on diatom surfaces. This will be subject of further AFM and particle tracking studies.
- Last, in contrast to previous SEM studies, high-resolution AFM images clearly show that the diatom frustule is built from silica nanoparticles. The size of these silica structures (nodules) varied (from 20 to

70 nm) on different layers. Both species show smaller silica nodules and the lower surface roughness on the inner layer than on the outer layer.

Acknowledgments This work is supported by funding from the Australian Research Council. We thank Adelaide Microscopy for use of their scanning electron microscopes.

References

1. C.R. Lowe, Curr. Opin. Struct. Biol. **10**, 428 (2000)
2. S.I. Stup, P.V. Braun, Science **277**, 142 (1997)
3. M. Sarikaya, C. Tamerler, A.K.Y. Jen, K. Scholten, F. Baneyx, Nat. Mater. **3**, 77 (2003)
4. E.G. Vrieling, T.P.M. Beelen, R.A. van Santen, W.W.C. Gieskes, J. Biotechnol. **70**, 39 (1999)
5. P. Ball, Nanotechnology **13**, 15 (2002)
6. J. Parkinson, R. Gordon, TiBTECH **17**, 190 (1999)
7. R.W. Drum, R. Gordon, TiBTECH **21**, 325 (2003)
8. T. Cordain, P.J. Lopez, ChemBioChem. **4**, 251 (2003)
9. M. Hilderbrand, Prog. Org. Coating **47**, 256 (2003)
10. G.R. Hasle, E.E. Syversten, in *Marine Diatoms: Identifying Marine Diatoms and Dinoflagellates*, ed. by K. Tomas (Academic Press, San Diego, 1996)
11. F. Noll, M. Sumper, N. Hampp, Nano Lett. **2**, 91 (2002)
12. R. Wetherbee, S. Craford, P. Mulvaney, in *Biomineralisation: From Biology to Biotechnology and Medical Application*, ed. by E. Beurlein (Wiley-VCH, Weinheim, 2000), p 189
13. K.H. Sandhage, M.B. Dickerson, P.M. Huseman, M.A. Carana, J.D. Clifton, T.A. Bull, T.J. Heibel, W.R. Overton, M.E.A. Shoenwaelder, Adv. Mater. **14**, 429 (2002)
14. S.B. Cheng, C.D. Skinner, J. Taylor, A. Attiya, W.E. Lee, G. Picelli, D.J. Harison, Anal. Chem. **73**, 1472 (2001)
15. D. Losic, J.G. Mitchell, N.H. Voelcker, Chem. Commun. 4905 (2005)
16. M.S. Hale, J.G. Mitchell, Aquat. Microb. Ecol. **24**, 287 (2001)
17. M.S. Hale, J.G. Mitchell, Nano Lett **1**, 617 (2001)
18. M.S. Hale, J.G. Mitchell, Nano Lett. **2**, 657 (2002)
19. G.J.M. Bruin, Electrophoresis **21**, 3931 (2000)
20. M. De Stefano, W.H.C.F. Kooistra, D. Marino, J. Phycol. **39**, 735 (2003)
21. E. Kiefer, L. Sigg, P. Schosseler, Environ. Sci. Technol. **31**, 759 (1997)
22. S.A. Craford, M.J. Higgins, P. Mulvaney, R. Wetherbee, J. Phycol. **37**, 543 (2001)
23. M.J. Higgins, J.E. Sader, P. Mulvaney, R. Wetherbee, J. Phycol. **39**, 722 (2003)
24. A. Linder, J. Colchero, H.J. Apell, O. Marti, J. Mlynek, Ultramicroscopy **42–44**, 329 (1992)
25. I.C. Gebeshuber, J.H. Kindt, J.B. Thompson, Y. Del Amo, H. Stachelberger, M.A. Brzezinski, G.D. Stucky, D.E. Morse, P.K. Hansma, J. Microsc. **212**, 292 (2003)
26. R. Lal, S.A. John, Am. J. Physiol. **266**, C1 (1994)
27. G. Massé, M. Poulin, S.T. Belt, J.M. Robert, A. Barreaus, Y. Rince, S.J. Rowland, J. Microsc. **204**, 87 (2001)
28. N. Almqvist, Y. Delamo, B.L. Smith, N.H. Thomson, A. Bartholdson, R. Lal, M. Brzezinski, P.K. Hansma, J. Microsc. **202**, 518 (2003)
29. R.R.L. Guillard, J.H. Ryther, Can. J. Microbiol. **8**, 229 (1962)
30. R. Hasle, G.A. Fryxell, Trans. Am. Microsc. Soc. **89**, 469 (1970)
31. D. Losic, K. Short, J.J. Gooding, J.G. Shapter, J. Serb. Chem. Soc. **69**, 93 (2004)
32. N. Kroger, R. Deutzmann, M. Sumper, J. Biol. Chem. **276**, 6066 (2001)
33. C.E. Hamm, R. Merkel, O. Springer, P. Jurkojc, C. Maler, K. Prechtel, V. Smatacek, Nature **421**, 841 (2003)
34. A. Janshoff, C. Steinem, N. Voelcker, V. Lin, M.R. Ghadiri, Tetrahedron **60**, 11259 (2004)